Editors' Suggestion

Single-Quantum-Dot Heat Valve

B. Dutta,[1] D. Majidi,[1] N. W. Talarico,[2] N. Lo Gullo,[2] H. Courtois,[1] and C. B. Winkelmann[1]
[1]Univ. Grenoble Alpes, CNRS, Grenoble INP, Institut Néel, 25 Avenue des Martyrs, 38042 Grenoble, France
[2]QTF Centre of Excellence, Turku Centre for Quantum Physics, Department of Physics and Astronomy, University of Turku, 20014 Turku, Finland

(Received 17 February 2020; revised 11 October 2020; accepted 21 October 2020; published 2 December 2020)

We demonstrate gate control of electronic heat flow in a thermally biased single-quantum-dot junction. Electron temperature maps taken in the immediate vicinity of the junction, as a function of the gate and bias voltages applied to the device, reveal clearly defined Coulomb diamond patterns that indicate a maximum heat transfer at the charge degeneracy point. The nontrivial bias and gate dependence of this heat valve results from the quantum nature of the dot at the heart of device and its strong coupling to leads.

DOI: 10.1103/PhysRevLett.125.237701

In the emerging field of quantum thermodynamics, heat transport and dissipation in a quantum electronic device is a fundamentally important topic [1–4]. Gate-tunable, single-quantum-dot junctions [5] are paradigmatic test benches for quantum transport. Whereas the study of charge transport therein has already allowed the exploration of a large palette of physical effects at play, heat transport and thermoelectric properties have been investigated in a limited number of cases, e.g., in quantum dots formed in a two-dimensional electron gas (2DEG) [6–9] and in semiconducting nanowires [10–12]. As opposed to charge transport processes, the understanding of electronic heat transport and generation across a nanoscale object is, experimentally, still in its infancy [13–15]. Local thermometry has been achieved only in a very limited number of quantum devices. The temperature dependence of the critical current of a superconducting weak link was used in scanning probe experiments to reveal, for instance, the scattering sites in high-mobility graphene [16,17]. Yet, to date, these experiments are limited to temperatures above 1 K. At mK temperatures, local thermometry can be performed in quantum devices formed in a 2DEG by a variety of methods [18,19] that have recently been pushed to quantitative accuracy [20–22]. Noise thermometry was applied to thermoelectric measurements in indium arsenide nanowires [23]. In metallic devices, electronic thermometry is usually based on the temperature dependence of charge transport in superconducting hybrids, either in the tunneling regime for normal metal-insulator-superconductor (NIS) junctions [24,25] or at higher transparencies allowing for superconducting correlations [26–28]. This has recently allowed the realization of a photonic heat valve with a superconducting qubit coupled to heat reservoirs (probed by NIS probes) through coplanar waveguide resonators [29].

The single electron transistor (SET) is an essential brick for the emerging field of quantum caloritronics [30]. Building on the NIS thermometry technique, the thermal conductance of a metallic SET was measured [31]. Despite the continuous density of states in the metallic island, electron interactions readily led to striking deviations from the Wiedemann-Franz law [32]. Going beyond this simple case, two questions arise: (i) how does such a SET behave thermally beyond equilibrium, that is, at finite voltage bias and/or at large temperature difference where both Joule heat and heat transport are to be taken into account, and (ii), if the central island is replaced by a quantum dot (QD), how would the discrete nature of its energy spectrum manifest in the thermal properties of the device? In the weak coupling regime, the discreteness of the QD energy spectrum makes electronic transport processes strongly selective in energy. At zero net particle current, whatever the gate voltage, the heat flow is zero since electrons tunnel back and forth exactly at the energy level defined by the QD. The heat conductance is thus zero at all gate voltages. Heat transfer is predicted only at nonzero particle current, when the QD energy level is positioned just above or below the Fermi level of the hot lead, so that high-energy electrons can escape through the dot, or low-energy electrons can be injected there [19,33].

In this Letter, we report on the operation of a single-quantum-dot heat valve. The methodological novelty is to introduce local thermometry in a metallic single-quantum-dot device. When current flows through it, Joule dissipation results in a temperature increase following the usual Coulomb diamond pattern. At zero net charge current and charge degeneracy, the observed electronic heat transfer is the result of energy quantization in the dot combined with strong tunnel coupling to the leads.

Figures 1(a) and 1(b) displays a colored scanning electron micrograph of a typical device like the one reported here, whereas Fig. 1(c) shows a thermal diagram of the same, with the corresponding color code for each device element. The device is different from that in

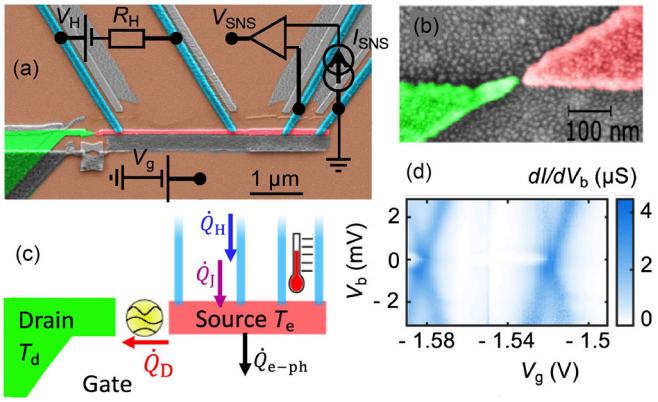

FIG. 1. A single-quantum-dot transistor integrating a local thermometer and a heater for heat transport measurement. (a) False-colored SEM image of a typical device. The source is colored in red, the drain in green, and the superconducting leads in blue. The circuit diagram shows the heat transport setup. The longer (2.5 μm) SNS junction is used as a heater driven by a constant d.c. battery and the shorter (700 nm) SNS junction is used as a thermometer. (b) Enlarged view of the nanogap between the "source" and "drain" created by electromigration and the nanoparticles made by Au evaporation. (c) Schematic of the device, with the different heat flows to and from the source. (d) Differential conductance map of the device measured at 70 mK against the drain-source bias voltage V_b and the gate voltage V_g with no additional heating applied.

Ref. [34], but it has the same geometry and the fabrication procedure is similar. The fabrication of the main part of the device is based on e-beam-lithography, three-angle, Au thin film evaporation and lift-off. After the lift-off, we deposit a 1–2 nm thin Au layer on top of the whole device. Because of the surface tension forces, this small amount of deposit leads to the formation of 5–10 nm diameter Au nanoparticles on the sample. A bow-tie shaped Pt electromigration junction forms the central part of the device on which the Au nanoparticles form a dense layer of QDs [see Fig. 1(b)]. Here we have chosen Pt as the electromigrated material in order to ensure the source local density of states at the QD contact to be free of superconducting correlations induced by the nearest Al lead [35].

The electromigration junction is connected on one side to a bulky drain electrode made of Au, in fairly good contact to the thermal bath at a temperature T_b, and on the other side to a narrow source electrode, again made of Au [34]. Four Al leads provide contacts to the source through a transparent interface. At temperatures well below the Al superconducting critical temperature, these leads are thermally insulating. The source is therefore fairly thermally decoupled from its environment. In the standard hot electron assumption, electron-electron equilibration is much faster than any other dynamical process. The source electrons are thus in a quasiequilibrium state described by a Fermi-Dirac distribution at a temperature T_e that can significantly differ from T_b. The pair of closely spaced Al leads connected to the source forms a superconductor-normal metal-superconductor (SNS) junction with a temperature-dependent critical current that will be used as an electronic thermometer. Conversely, the widely spaced pair of Al leads forms instead a junction with a vanishing critical current, which allows it to be used as an ohmic heater. In contrast to prior work [31], we have chosen here transparent rather than tunnel contacts to the source for two reasons. First, SNS junctions can provide less invasive thermometers than NIS junctions that are biased at a voltage of about Δ/e, which in turn can lead to significant heating and cooling effects [25]. Second, electromigration requires low access resistances, which is inherently incompatible with tunnel contacts.

The nanometer-sized gap was created within the Pt constriction by means of electromigration at a temperature of 4 K [34,36]. The device was further cooled *in situ* down to the cryostat base temperature of about 70 mK. Figure 1(d) shows a differential conductance map of the QD junction as a function of bias and gate voltages V_b and V_g, respectively, with no additional heating. From the observed Coulomb diamonds, one finds a charging energy $E_c = 4$ meV [37]. Our detailed analysis [38] provides a tunnel coupling $\hbar\Gamma$ value in the range 0.2–1.5 meV, depending on the considered single energy level involved in low-bias electron transport at a given charge degeneracy point. In spite of the large tunnel coupling $\hbar\Gamma \gg k_B T$, it is still not strong enough to induce a Kondo effect.

We now move to the description of the electron thermometers. The critical current I_C of an SNS junction is highly sensitive to the electronic temperature T_e in N. The relevant energy scale is the Thouless energy $\epsilon_{\rm th} = \hbar D/L^2$, where D is the diffusion constant in N and L is the junction length [45]. For $T_e > \epsilon_{\rm th}/k_B$, I_C decreases rapidly with increasing temperature, allowing it to be used as a secondary electron thermometer [26,27]. In a single IV characteristic, the switching current is defined as the value of the current at which the voltage is larger than a threshold voltage chosen above the measurement noise level. Figure 2(a) shows a series of such characteristics at different bath temperatures. Switching current histograms, together with a Gaussian fit of their envelope, are shown in Fig. 2(c) for a series of bath temperature values. The histogram width increases with the temperature, consistent with a Josephson energy fluctuating by $2k_B T$. In Fig. 2(b), the variation of the critical current with the bath temperature fits nicely the theoretical expectation [45], the latter being used as the thermometer calibration. The low Thouless energy $\epsilon_{\rm th} \sim 5$ μeV was chosen in order to avoid a saturation of I_C. The thermometer thus remains sensitive at low temperature, where thermal transport through the QD gains importance compared to other heat relaxation processes.

In the experiment, we heat up the source by applying a constant heating power $\dot{Q}_H = 6$ fW to the heater junction. The drain is biased at a potential V_b, the source side being

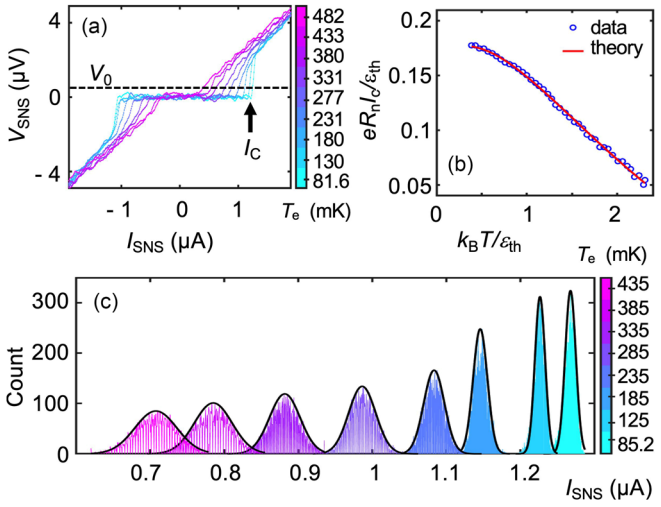

FIG. 2. Characterization of the SNS thermometer. (a) d.c. IV characteristics of the SNS thermometer junction at different bath temperature T_b, the current bias value at which the voltage exceeds a threshold $V_0 \simeq 0.5\ \mu$V defining the switching current. (b) The critical current I_C as a function of the bath temperature, the axes being normalized. It is defined as the most probable switching current extracted from the histograms. The calibration curve (red solid line) is a fit with the theory [45]. (c) Histogram of the stochastic switching current of the SNS junction at different bath temperatures with a fitted Gaussian envelope for each.

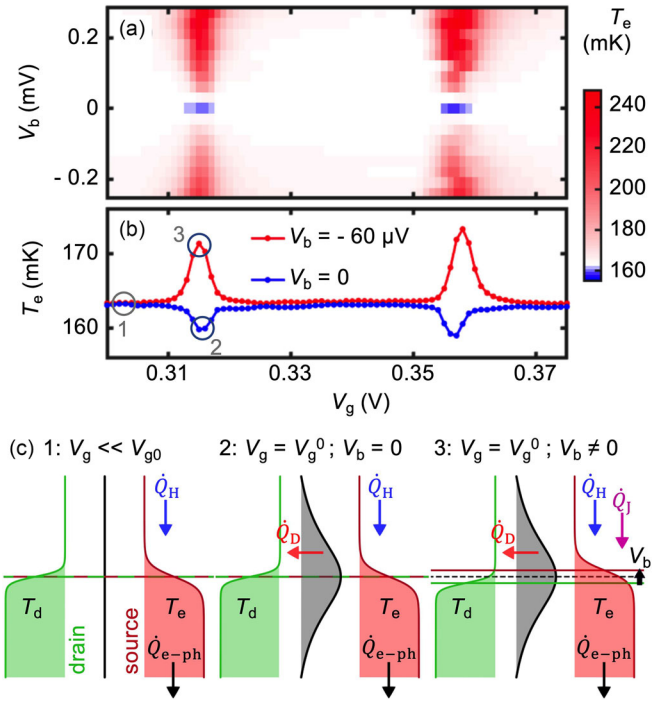

FIG. 3. Competition between thermal transport and dissipation across the QD junction. (a) Experimental map of the source electronic temperature in the $V_b - V_g$ plane. (b) Individual gate traces of the source temperature at two different bias values. (c) Schematic energy diagram of the heat flows in and out of the source in various conditions as indicated by labels in (b): (1) away from charge degeneracy and at zero bias (left), (2) at a charge degeneracy point $V_g = V_g^0$ but still at zero bias (middle), or (3) at nonzero bias in a conducting region (right). The gray profile depicts the quantum level spectral density. The ratio between the level broadening $\hbar\Gamma$, the bias V_b, and the thermal energy k_BT are in correspondence with panel (b) conditions. The arrows indicate the applied heating power $\dot{Q}_H$, the Joule power $\dot{Q}_J$, the electron-phonon coupling power $\dot{Q}_{\text{e-ph}}$ and the power flow through the QD $\dot{Q}_D$.

grounded via one of the SNS thermometer contacts. Figure 3(a) shows a map of the source electronic temperature as a function of V_b and V_g. Its resemblance to the charge conductance map of Fig. 1(d) is striking. The source temperature T_e increases rapidly with increasing charge current due to the related Joule power. Right at the charge degeneracy point, the source temperature is lower than in the rest of the map. The higher resolution temperature map of Fig. 4(a) shows a clear cooling region of ellipsoidal shape with slightly canted axes. This cooling effect is the result of the enhanced heat transfer between the hot source and cold drain.

Figure 3(c) shows energy diagrams for three different cases indicated by circles in the temperature $T_e(V_g)$ profiles at two different bias of Fig. 3(b). At zero bias and far away from charge degeneracy (case 1), there is neither Joule power nor heat flow through the QD. The source is overheated up to $T_e = 163.5$ mK due to the balance between the applied power $\dot{Q}_H$ and the main thermal leakage channel, namely the electron-phonon coupling $\dot{Q}_{\text{e-ph}}$. Still at zero bias but near a charge degeneracy point (case 2), there is a heat flow $\dot{Q}_D$ through the QD but still no charge flow. This shows up [blue curve in Fig. 3(b)] as a temperature T_e drop by several mK at the charge degeneracy point. The gate-controlled QD junction thus acts as a heat valve. At higher bias (case 3), this cooling contribution is overcome by the Joule heat $\dot{Q}_J$. A temperature maximum is thus observed at values of the gate potential close to the charge degeneracy point [red curve in Fig. 3(b)].

The mere observation of cooling at the charge degeneracy point is in clear contradiction to the theoretical prediction in the weak coupling, sequential tunneling regime. Indeed the present experiment deals with a strong tunnel coupling between the QD and the leads, with a ratio $\hbar\Gamma/k_BT_e \approx 20$, rendering the weak coupling picture inapplicable.

We now go beyond the sequential tunneling approximation. Thanks to the extremely high charging energy, in the vicinity of a charge degeneracy point, the device can be described as a noninteracting single energy level. We are interested in exploring the properties of the leads at stationarity and in particular their electronic temperature; in the nonequilibrium Green's functions framework, this is possible via the so-called inbedding technique [38,46,47]. The latter is not based on a full heat balance model accounting for the heat flow via phonons and the superconducting leads. We instead assume that the electron-phonon coupling strength itself does not change appreciably within the temperature range of the map, which is

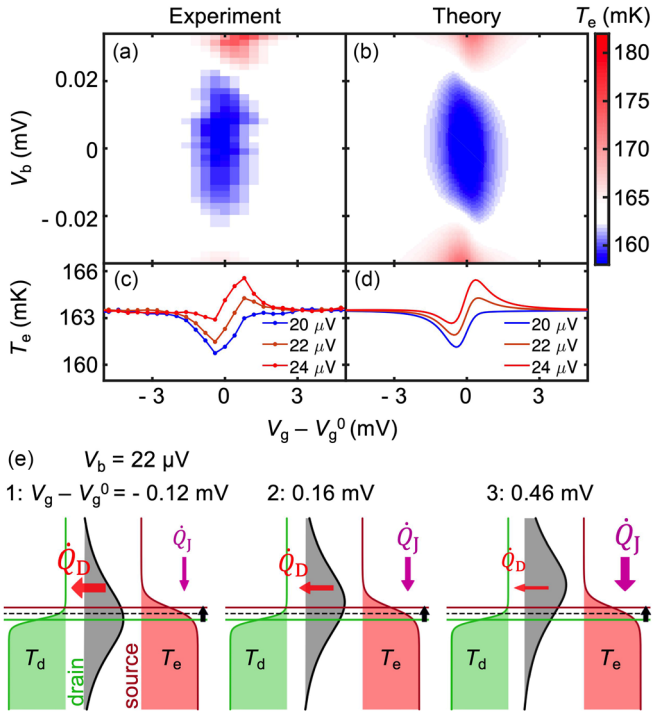

FIG. 4. Quantum dot heat valve. (a) A highly resolved map of the source electronic temperature at the same experimental condition as in Fig. 3 and around a charge degeneracy point defined by $V_g = V_g^0$. (b) Calculated temperature map obtained with the inbedding technique with $\Gamma = 0.25$ meV, $\Gamma_L/\Gamma_R = 3/17$, and $T_d = 85$ mK. (c) Experimental and (d) theoretical variation of the temperature in the region where crossing from cooling to heating is observed; each curve refers to a given applied bias V_b: (blue) 20 μV, (orange) 22 μV, (red) 24 μV. (e) Schematics describing the crossover between the heat flow $\dot{Q}_D$ and the Joule heat $\dot{Q}_J$ as a function of the gate at a fixed bias, resulting in temperature decrease at $V_g - V_g^0 = -0.12$ mV (case 1, left) or increase at 0.46 mV (3, right). At 0.16 mV (2, middle), the two flows are equilibrated. The electron-phonon heat $\dot{Q}_{\text{e-ph}}$ as well as the injected heat $\dot{Q}_H$ are omitted for clarity. The widths of the arrows indicate their relative strengths.

equivalent to assuming that the main particle and energy redistribution processes in the lead are dominated by electron-electron interactions. By including in the theory the measured temperature (163.5 mK) of the source when decoupled from the QD, we effectively take into account its thermal coupling to the bath.

The theoretical temperature map around a charge degeneracy point is shown in Fig. 4(b) and reveals a nice agreement with the experimental data in Fig. 4(a). Here, the temperature of the drain T_d is set to 85 mK and the coupling of the QD to the drain is asymmetric with a coupling ratio $\Gamma_L/\Gamma_R = 3/17$ between left and right leads and $\Gamma = 0.25$ meV. These best fit values allow us to reproduce semiquantitatively the temperature profiles of the crossing region [see Figs. 4(c) and 4(d)]. The width of the cooling region along the gate potential axis is independent of the bath temperature and increases with the coupling Γ [38]. Conversely, its extension in bias depends weakly on Γ and increases with the temperature difference across the junction.

The present case actually has some similarities with the regime of a metallic SET where cooling at the charge degeneracy point was also found [32,34]. Nevertheless, an asymmetry in gate voltage is clearly observed in the experimental and theoretical temperature map. For a bias voltage V_b around 22 μV, the source temperature can be tuned either below or above the reference temperature of 163.5 mK by acting on the gate voltage [see Fig. 4(c)]. This behavior is not to be expected in the case of a metallic island where electron-hole symmetry in the density of states makes transport properties symmetric across the charge degeneracy point. Therefore, it is an unambiguous signature of the QD discrete energy spectrum. At a given bias, the value of the gate potential determines the position of the broadened energy level in the QD [see the gray profile in Fig. 4(e)] and thus the mean energy of the tunneling electrons. This in turn affects the heat balance in the source and modifies the boundary of the cooling region in the temperature map. The extension in bias of this crossover zone, where one can switch from cooling to heating by adjusting the gate, depends on both the coupling Γ and the temperature difference across the QD [38].

This work shows that electronic heat transport through a QD junction can be modulated by a gate potential, making it act as a gate-tunable heat valve. This behavior can have important consequences in the practical thermoelectric efficiency of such a single-quantum-dot junction [48]. The Coulomb diamond patterns in the temperature maps reveal the intimate relation between charge conductance on one hand and heat transport and dissipation on the other. Further experiments may allow a quantitative comparison of thermal effects to the charge transport properties in a wide range of tunnel couplings. The ability of precision electron thermometry at the heart of a QD-based device demonstrated here opens wide perspectives in the field of heat transport and dissipation in quantum electronic devices, paving the way for quantitative tests of the Landauer principle in the quantum information regime [49].

The authors thank B. Karimi and J. P. Pekola for stimulating discussions. Samples were realized at the Nanofab platform at Institut Néel with the help of T. Crozes. We acknowledge support from the Nanosciences Foundation under the auspices of the Foundation UGA and from the European Union under the Marie Skłodowska-Curie Grant Agreement No. 766025. N. L. G. and W. N. T. acknowledge support from the Academy of Finland Center of Excellence program (Project No. 312058) and the Academy of Finland (Project No. 287750). N. L. G. acknowledges funding from the Maupertuis Program for an RSM grant and from the Turku Collegium for Science and Medicine. Numerical simulations were performed at the Finnish CSC facilities under Project No. 2000962.

[1] E. Pop, Energy dissipation and transport in nanoscale devices, Nano Res. **3**, 147 (2010).

[2] W. Lee, K. Kim, W. Jeong, L. Zotti, F. Pauly, J. C. Cuevas, and P. Reddy, Heat dissipation in atomic-scale junctions, Nature (London) **498**, 209 (2013).

[3] L. Zotti, M. Bürkle, F. Pauly, W. Lee, K. Kim, W. Jeong, Y. Asai, P. Reddy, and J. C. Cuevas, Heat dissipation and its relation to thermopower in single-molecule junctions, New J. Phys. **16**, 015004 (2014).

[4] Y. Dubi and M. Di Ventra, Heat flow and thermoelectricity in atomic and molecular junctions, Rev. Mod. Phys. **83**, 131 (2011).

[5] L. P. Kouwenhoven, D. G. Austing, and S. Tarucha, Few-electron quantum dots, Rep. Prog. Phys. **64**, 701 (2001).

[6] R. Scheibner, H. Buhmann, D. Reuter, M. N. Kiselev, and L. W. Molenkamp, Thermopower of a Kondo Spin-Correlated Quantum Dot, Phys. Rev. Lett. **95**, 176602 (2005).

[7] R. Scheibner, M. König, D. Reuter, A. D. Wieck, C. Gould, H. Buhmann, and L. W. Molenkamp, Quantum dot as thermal rectifier, New J. Phys. **10**, 083016 (2008).

[8] S. F. Godijn, S. Möller, H. Buhmann, L. W. Molenkamp, and S. A. van Langen, Thermopower of a Chaotic Quantum Dot, Phys. Rev. Lett. **82**, 2927 (1999).

[9] A. S. Dzurak, C. G. Smith, C. H. W. Barnes, M. Pepper, L. Martĩn-Moreno, C. T. Liang, D. A. Ritchie, and G. A. C. Jones, Thermoelectric signature of the excitation spectrum of a quantum dot, Phys. Rev. B **55**, R10197 (1997).

[10] M. Josefsson, A. Svilans, A. M. Burke, E. A. Hoffmann, S. Fahlvik, C. Thelander, M. Leijnse, and H. Linke, A quantum-dot heat engine operating close to the thermodynamic efficiency limits, Nat. Nanotechnol. **13**, 920 (2018).

[11] G. Jaliel, R. K. Puddy, R. Sanchez, A. N. Jordan, B. Sothmann, I. Farrer, J. P. Griffiths, D. A. Ritchie, and C. G. Smith, Experimental Realization of a Quantum Dot Energy Harvester, Phys. Rev. Lett. **123**, 117701 (2019).

[12] D. Prete, P. A. Erdman, V. Demontis, V. Zannier, D. Ercolani, L. Sorba, F. Beltram, F. Rossella, F. Taddei, and S. Roddaro, Thermoelectric conversion at 30 K in InAs/InP nanowire quantum dots, Nano Lett. **19**, 3033 (2019).

[13] P. Kim, L. Shi, A. Majumdar, and P. L. McEuen, Thermal Transport Measurements of Individual Multiwalled Nanotubes, Phys. Rev. Lett. **87**, 215502 (2001).

[14] Z. Huang, F. Chen, R. D'Agosta, P. A. Bennett, M. Di Ventra, and N. Tao, Local ionic and electron heating in single-molecule junctions, Nat. Nanotechnol. **2**, 698 (2007).

[15] M. Tsutsui, M. Taniguchi, and T. Kawai, Local heating in Metal–Molecule–Metal junctions, Nano Lett. **8**, 3293 (2008).

[16] D. Halbertal, J. Cuppens, M. Ben Shalom, L. Embon, N. Shadmi, Y. Anahory, H. R. Naren, J. Sarkar, A. Uri, Y. Ronen, Y. Myasoedov, L. S. Levitov, E. Joselevich, A. K. Geim, and E. Zeldov, Nanoscale thermal imaging of dissipation in quantum systems, Nature (London) **539**, 407 (2016).

[17] A. Marguerite, J. Birkbeck, A. Aharon-Steinberg, D. Halbertal, K. Bagani, I. Marcus, Y. Myasoedov, A. K. Geim, D. J. Perello, and E. Zeldov, Imaging work and dissipation in the quantum Hall state in graphene, Nature (London) **575**, 628 (2019).

[18] L. W. Molenkamp, Th. Gravier, H. van Houten, O. J. A. Buijk, M. A. A. Mabesoone, and C. T. Foxon, Peltier Coefficient and Thermal Conductance of a Quantum Point Contact, Phys. Rev. Lett. **68**, 3765 (1992).

[19] J. R. Prance, C. G. Smith, J. P. Griffiths, S. J. Chorley, D. Anderson, G. A. C. Jones, I. Farrer, and D. A. Ritchie, Electronic Refrigeration of a Two-Dimensional Electron Gas, Phys. Rev. Lett. **102**, 146602 (2009).

[20] S. Jézouin, F. D. Parmentier, A. Anthore, U. Gennser, A. Cavanna, Y. Jin, and F. Pierre, Quantum limit of heat flow across a single electronic channel, Science **342**, 601 (2013).

[21] E. Sivre, A. Anthore, F. D. Parmentier, A. Cavanna, U. Gennser, A. Ouerghi, Y. Jin, and F. Pierre, Heat Coulomb blockade of one ballistic channel, Nat. Phys. **14**, 145 (2018).

[22] M. Banerjee, M. Heiblum, V. Umansky, D. E. Feldman, Y. Oreg, and A. Stern, Observation of half-integer thermal Hall conductance, Nature (London) **559**, 205 (2018).

[23] E. S. Tikhonov, D. V. Shovkun, D. Ercolani, F. Rossella, M. Rocci, L. Sorba, S. Roddaro, and V. S. Khrapai, Noise thermometry applied to thermoelectric measurements in InAs nanowires, Semicond. Sci. Technol. **31**, 104001 (2016).

[24] M. Nahum and J. M. Martinis, Ultrasensitive hot electron microbolometer, Appl. Phys. Lett. **63**, 3075 (1993).

[25] F. Giazotto, T. T. Heikkilä, A. Luukanen, A. M. Savin, and J. P. Pekola, Opportunities for mesoscopics in thermometry and refrigeration: Physics and applications, Rev. Mod. Phys. **78**, 217 (2006).

[26] M. Meschke, J. T. Peltonen, H. Courtois, and J. P. Pekola, Calorimetric readout of a superconducting proximity-effect thermometer, J. Low Temp. Phys. **154**, 190 (2009).

[27] L. B. Wang, O. P. Saira, and J.-P. Pekola, Fast thermometry with a proximity Josephson junction, Appl. Phys. Lett. **112**, 013105 (2018).

[28] F. Giazotto and M. J. Martĩnez-Perez, The Josephson heat interferometer, Nature (London) **492**, 401 (2012).

[29] A. Ronzani, B. Karimi, J. Senior, C. Chen, and J. P. Pekola, Tunable photonic heat transport in a quantum heat valve, Nat. Phys. **14**, 991 (2018).

[30] O. P. Saira, M. Meschke, F. Giazotto, A. M. Savin, M. Möttönen, and J. P. Pekola, Heat Transistor: Demonstration of Gate-Controlled Electronic Refrigeration, Phys. Rev. Lett. **99**, 027203 (2007).

[31] B. Dutta, J. T. Peltonen, D. S. Antonenko, M. Meschke, M. A. Skvortsov, B. Kubala, J. König, C. B. Winkelmann, H. Courtois, and J. P. Pekola, Thermal Conductance of a Single-Electron Transistor, Phys. Rev. Lett. **119**, 077701 (2017).

[32] B. Kubala, J. König, and J. Pekola, Violation of the Wiedemann-Franz Law in a Single-Electron Transistor, Phys. Rev. Lett. **100**, 066801 (2008).

[33] H. L. Edwards, Q. Niu, and A. L. de Lozanne, A quantum dot refrigerator, Appl. Phys. Lett. **63**, 1815 (1993).

[34] B. Dutta, D. Majidi, A. Garcia Corral, P. A. Erdman, S. Florens, T. A. Costi, H. Courtois, and C. B. Winkelmann, Direct probe of the Seebeck coefficient in a Kondo-correlated single-quantum-dot transistor, Nano Lett. **19**, 506 (2019).

[35] T. Kontos, M. Aprili, J. Lesueur, X. Grison, and L. Dumoulin, Superconducting Proximity Effect at the Paramagnetic-Ferromagnetic Transition, Phys. Rev. Lett. **93**, 137001 (2004).

[36] H. Park, A. K. Lim, A. P. Alivisatos, J. Park, and P. L. McEuen, Fabrication of metallic electrodes with nanometer separation by electromigration, Appl. Phys. Lett. **75**, 301 (1999).

[37] Here we use the definition $E_c = e^2/2C_\Sigma$ where C_Σ is the total capacitance of the dot with respect to leads and gate.

[38] See Supplemental Material at http://link.aps.org/supplemental/10.1103/PhysRevLett.125.237701 where we discuss about the sample fabrication, charge transport properties, performance of our SNS thermometer junction as a bolometric detector, and the details of the theoretical approach used to explain our data, which includes Refs. [39–44].

[39] K. I. Bolotin, F. Kuemmeth, A. N. Pasupathy, and D. C. Ralph, Metal-nanoparticle single-electron transistors fabricated using electromigration, Appl. Phys. Lett. **84**, 3154 (2004).

[40] D. C. Ralph, C. T. Black, and M. Tinkham, Spectroscopic Measurements of Discrete Electronic States in Single Metal Particles, Phys. Rev. Lett. **74**, 3241 (1995).

[41] D. M. T. van Zanten, F. Balestro, H. Courtois, and C. B. Winkelmann, Probing hybridization of a single energy level coupled to superconducting leads, Phys. Rev. B **92**, 184501 (2015).

[42] J. M. Thijssen and H. S. J. van der Zant, Charge transport and single-electron effects in nanoscale systems, Phys. Status Solidi (b) **245**, 1455 (2008).

[43] E. Bonet, M. M. Deshmukh, and D. C. Ralph, Solving rate equations for electron tunneling via discrete quantum states, Phys. Rev. B **65**, 045317 (2002).

[44] J. T. Peltonen, P. Virtanen, M. Meschke, J. V. Koski, T. T. Heikkilä, and J. P. Pekola, Thermal Conductance by the Inverse Proximity Effect in a Superconductor, Phys. Rev. Lett. **105**, 097004 (2010).

[45] P. Dubos, H. Courtois, B. Pannetier, F. K. Wilhelm, A. D. Zaikin, and G. Schön, Josephson critical current in a long mesoscopic S-N-S junction, Phys. Rev. B **63**, 064502 (2001).

[46] G. Stefanucci and R. van Leeuwen, *Nonequilibrium Many-Body Theory of Quantum Systems* (Cambridge University Press, Cambridge, England, 2013).

[47] N. W. Talarico, S. Maniscalco, and N. L. Gullo, Study of the energy variation in many-body open quantum systems: Role of interactions in the weak and strong coupling regimes, Phys. Rev. B **101**, 045103 (2020).

[48] A. Harzheim, J. K. Sowa, J. L. Swett, G. A. D. Briggs, J. A. Mol, and P. Gehring, Role of metallic leads and electronic degeneracies in thermoelectric power generation in quantum dots, Phys. Rev. Research **2**, 013140 (2020).

[49] J. P. Pekola, Towards quantum thermodynamics in electronic circuits, Nat. Phys. **11**, 118 (2015).